Contents lists available at ScienceDirect

Microelectronic Engineering

journal homepage: www.elsevier.com

Research paper

Effect of deposition angle on fabrication of plasmonic gold nanocones and nanodiscs

Jiří Liška [a, *], Filip Ligmajer [a, b], Pedro V. Pinho N [c], Lukáš Kejík [a, b], Michal Kvapil [a, b], Petr Dvořák [a, b], Nikolaus S. Leitner [d], Erik Reimhult [d], Tomáš Šikola [a, b]

[a] Central European Institute of Technology, Brno University of Technology, Purkyňova 123, 612 00 Brno, Czech Republic
[b] Institute of Physical Engineering, Faculty of Mechanical Engineering, Brno University of Technology, Technická 2, 616 69 Brno, Czech Republic
[c] Institute of Physics "Gleb Wataghin", University of Campinas, R. Sérgio Buarque de Holanda, 777 - Cidade Universitária, 13083-859 Campinas, SP, Brazil
[d] Department of Nanobiotechnology, University of Natural Resources and Life Sciences, Muthgasse 11-II, A-1190 Vienna, Austria

ARTICLE INFO

Keywords:
Nanocone
Nanodisc
Optical antenna
Electron beam evaporation
Electron beam lithography
Plasmonics

ABSTRACT

Metal nanocones can exhibit several strong plasmonic resonances, which are associated with intense and accessible electromagnetic hot spots. They can thus be used to enhance light–matter interactions or to facilitate location-specific sensing while enabling separation of some non-specific contributions towards the sensing signal. Nanocones and similar 3D structures are often fabricated with the use of the so-called self-shading effect, which occurs during the evaporation of a metal film into circular nanowells. Unfortunately, a full description of a successful deposition process with all the essential details is currently missing in literature. Here we present a detailed view of the fabrication of ordered arrays of conical gold nanostructures using electron beam lithography and gold electron beam evaporation. We show that the symmetry of the fabricated nanostructures is influenced by the lateral position of the substrate on the sample holder during the deposition. Off-axis deposition or tilt of the sample leads to asymmetric nanostructures. When the deposited film is thick enough, or the nanowells narrow enough, the entrance aperture is clogged, and nanocones with sharp tips are formed. In contrast, flat-top truncated cones are produced for thinner films or wider nanowells. All these findings help to identify inherent limits for the production of wafer-scale arrays of such non-planar nanostructures. On the other hand, they also suggest new fabrication possibilities for more complicated structures such as mutually connected nanocones for electrically addressable chips.

1. Introduction

Localized surface plasmon resonance of metal nanostructures is a highly studied topic, with plenty of applications such as heat-assisted magnetic recording [1], imaging below the diffraction limit [2], construction of metasurfaces [3], or biosensing [4]. The size and shape of nanostructures are the key aspects that define the optimal building blocks for the respective applications. These range from simple discs or cuboids in planar geometries [5] to 3D nanostructures having chiral [6] or other sophisticated shapes [7]. One large class of the 3D nanostructures are metal nanocones. They offer several unique features like highly accessible hotspots exposed to the environment or different resonant modes connected with different excitation and collection geometries. The intense and accessible hotspots of nanocones have been utilized in surface-enhanced Raman spectroscopic studies [8–10], photoluminescence studies of energy transfer between plasmonic antennas and quantum dots [11,20,21]. They have been used in scanning-probe near-field optical microscopy, where sharp tips and nanocones are the fundamental building blocks [12–14]. Metal nanocones also seem like a promising platform for location-specific biosensors. The presence of a target analyte near the tip of the nanocone results in a characteristic spectral shift of the relevant plasmonic mode, while when the analyte resides near the base of the nanocone, a different plasmonic mode is affected, and thus the two analyte locations can be distinguished [15–19]. This was used to study molecular assembly [15], detect analytes at conventional [8] or even very low [33] concentrations, and to analyze cell lysate [10]. Single-molecule sensing with this platform was also proposed theoretically [16].

Metal nanocones can be fabricated by several top-down or bottom-up strategies, each of them having its natural advantages and weaknesses: Focused ion beam milling or electron beam induced deposition of metals both allow very accurate control of the shape and locations

* Corresponding author.
Email address: jiri.liska@ceitec.vutbr.cz (J. Liška)

https://doi.org/10.1016/j.mee.2020.111326
Received 11 February 2020; Received in revised form 12 April 2020; Accepted 15 April 2020
Available online xxx
0167-9317/

of the nanocones [20–22]. However, they are inherently slow techniques and thus unsuitable for the fabrication of nanostructures over large areas. Dry etching of metal films through a nanostructured mask is fundamentally similar to focused ion beam milling, yet it is a much faster process. With the dry etching, large areas of nanocones can be produced on planar or even non-planar surfaces [10,18,23–30]. The third fabrication strategy is based on the self-formation of nanocones inside cylindrical nanowell templates during the deposition of the respective metal, making use of an effect which is known as aperture clogging or self-shading [15,23,31,32]. The gradual deposition of a metal onto the sidewalls and the top face of the mask aperture leads to a decrease of its effective size and to the formation of cone-shaped nanostructures beneath the aperture (see Fig. 1).

Either the deposited nanocones can remain inside the resulting metal cavities [33] or one can remove these metal and resist layers using a lift-off process, which will then lead to free-standing nanocones. If the nanowell templates are prepared inside inorganic dielectrics like silicon nitride or silicon dioxide, the resulting nanocones will end up buried inside the nanowells. These structures can be used in biosensing experiments, where the inherent barrier of the nanowell orifice blocks unwanted interactions of large blocks of matter with the sensing nanocone elements [15,34,35]. The self-shading effect works for nanowells prepared by all sorts of lithographic procedures: Large areas randomly covered by nanocones can be prepared very quickly by colloidal or so-called hole-mask lithography [23]. Wafer-scale arrays of precisely positioned and shaped nanocones can be achieved by nanoimprint lithography [8,36–39] or by ultraviolet laser interference lithography [40]. Electron beam lithography (EBL) cannot surpass the aforementioned techniques in terms of speed, but it is very versatile and can produce a wide range of nanocone patterns. The shapes of the resulting nanostructures can then be controlled by modifications of the lithographic design, e.g. from circular to complex structures like a pair of circles connected with a narrow line, which allows obtaining interesting 3D objects like bridged nanocones [41], winged nanocones [42], or L-shaped structures [37].

Despite the richness of various metal nanocone platforms mentioned above, we want to bring attention to one problematic aspect of the self-shading process. Imperfect planar alignment of the substrate during deposition or the inherent multi-directionality of physical vapor deposition methods lead to a broken symmetry of the nanocones fabricated on large-scale substrates. These asymmetries are directly related to the position on the sample holder. They are hardly visible in the conventional top-view electron microscopy imaging and can, therefore, often be missed during brief post-fabrication inspections. The details of the fabrication process described here will help to better understand the essential aspects of the self-shading mechanism, which plays a role even in the fabrication of simple flat nanodiscs. This knowledge can also be utilized for the fabrication of complex interconnected nanocone structures suitable for electrically addressable chips.

2. Methods

2.1. Fabrication of samples

Silicon substrates (Siegert Wafer GmbH) were cleaned by acetone and isopropyl alcohol, spin-coated with 300 nm of positive tone electron beam resist (CSAR 62/AR-P 6200.09, Allresist GmbH), and baked out at 150 °C on a hotplate for 1 min. No adhesion promoter was used. Hexagonal arrays of circular nanowells with nominal diameters of 50, 100 and 200 nm and various spacings (the gap between structures of 300, 500, 1000 nm) were patterned by EBL using a scanning electron microscope (SEM, MIRA3, Tescan, equipped with a laser interferometer stage RAITH), with an accelerating voltage of 30 kV and probe current of 25 pA (further information on the EBL process is provided in the Supplementary Data, Sect. 1). After the standard developing procedure (developer AR 600–546 for 1 min, stopper AR 600–60 for 30s, demineralized water for 30s), the resist was stripped in O_2 plasma for 20 s (PlasmaPro NGP 80, Oxford Instruments Ltd., pressure 40 mTorr, power 50 W, DC bias voltage 245 V). The resulting nanowells in the developed resist had the same diameters as the nominal values, i.e. 50 nm, 100 nm, and 200 nm (corresponding to the height–diameter aspect ratio of 6, 3, and 1.5, respectively). Nanowells in the resist were then covered by a 5 nm thin titanium adhesion layer and by a 245 nm thick gold film in an ultra-high vacuum electron beam evaporator (Bestec GmbH). Note, that a proper deposition rate is crucial to get the desired nanocone shape — it must be kept above 1.5 Å/s to get conical structures; at lower values, structures with different morphology, like spinning-top or bowl shapes, are formed [8]. Therefore, the rate of gold deposition was held above this limit at 2.2 Å/s. Finally, the lift-off process was performed in a common CSAR remover (AR 600–71, Allresist, 15 h bath and subsequent ultrasound).

3. Results and discussion

To study the influence of the sample position during the deposition, we mounted the lithographically patterned substrates onto different lateral positions of the sample holder inside the deposition chamber (see Fig. 2, center) with distances from the center of the holder in the range of 0–105 mm. The holder was perpendicular to the deposition beam, 400 mm away from the crucible. The flux incidence angles (the local deposition angles) on the samples were therefore in the range of 0–15° (schema in Fig. SD2a, the Supplementary Data). Inspection of the resulting structures in SEM after the lift-off showed that the most symmetric structures of the highest quality were formed on the substrates located at the center of the holder with a corresponding flux in-

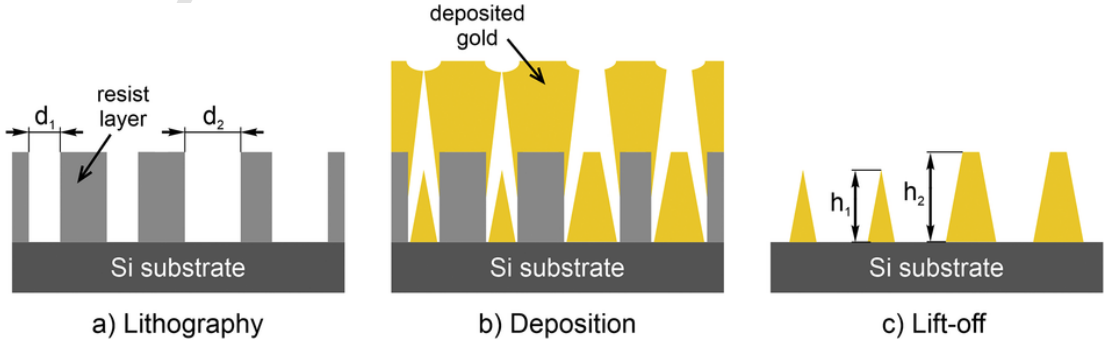

Fig. 1. Schematic of the fabrication process of metal nanocones. (a) A matrix of circular nanowells with two diameters is fabricated by electron beam lithography into a polymer resist on top of a silicon substrate. (b) The metal nanocones are formed inside the nanowells via the self-shading effect during metal evaporation. (c) The free-standing structures on the substrate are formed after the lift-off, when the resist and surrounding metal are removed.

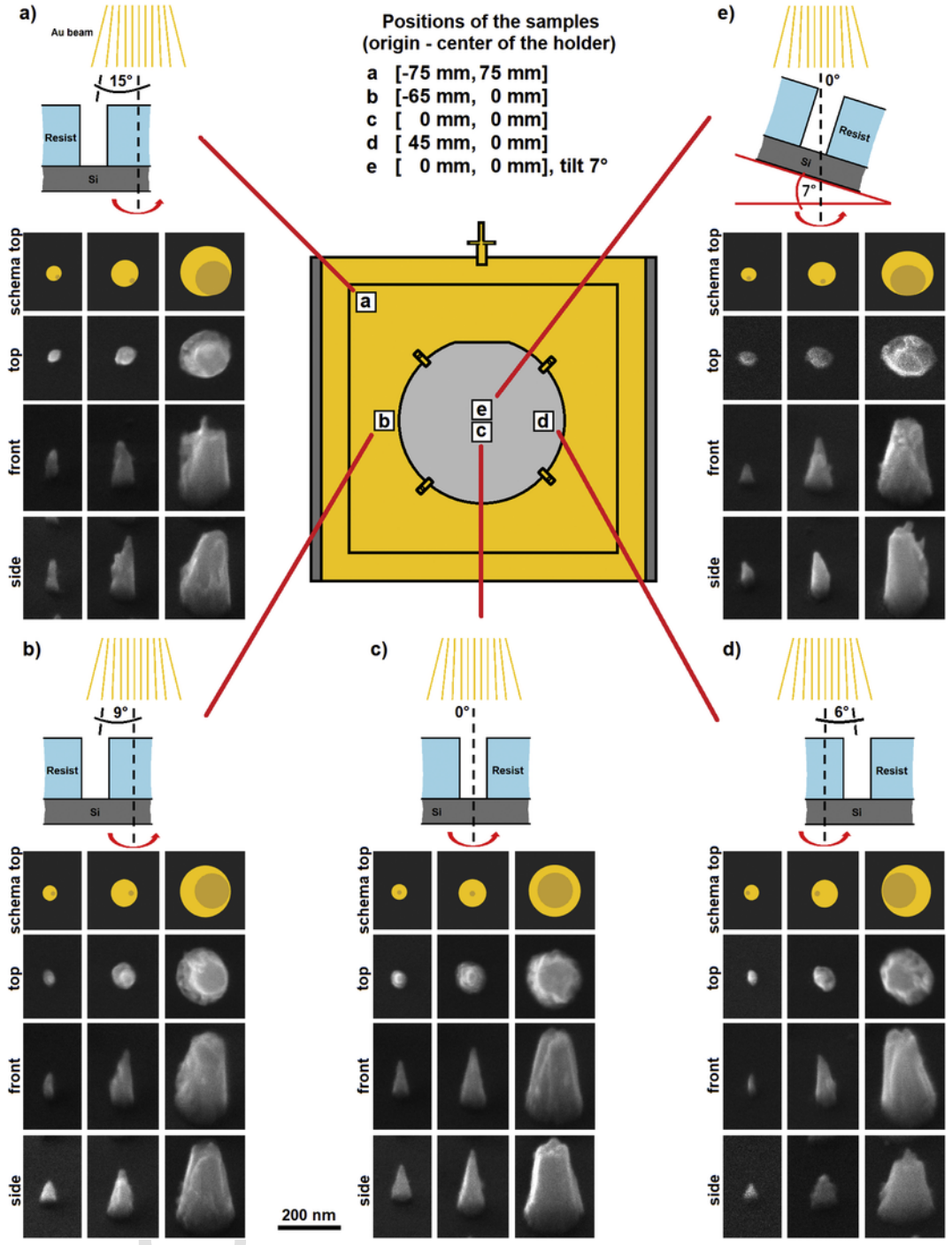

Fig. 2. The shape of nanocones with 50, 100 and 200-nm diameter in SEM (LYRA3, MIRA3, Tescan) under the top, front and side view (tilt of 55°) together with the schema of deposition geometry and sample arrangement on the evaporator holder with a 4-inch wafer in the center. Samples were placed at the total distance from the center holder and under flux incidence angle as follows: a) 105 mm, 15° (schema rotated by 45°), b) 65 mm, 9°, c) 0 mm, 0°, d) 45 mm, 6°, e) 0 mm, 0° and sample tilt of 7° (schema rotated by 90°).

cidence angle of 0° (Fig. 2c, their parameters are summarized in Table 1). Smaller nanowells with 50 nm and 100 nm diameters ended up with sharp nanocones having the height–diameter aspect ratio close to 2:1. As the total thickness of the deposited metal was only 250 nm, nanowells with the 200 nm diameter were too wide to get clogged during the deposition. Therefore, truncated nanocones were formed. The thickness of the deposited gold film thus, in our case, had to be at least 400 nm (twice as large as the diameter of the largest nanowells) to ensure the production of sharp nanocones even with the 200 nm diameter.

When the substrates were placed out of the center of the sample holder during the deposition with the corresponding flux incidence angles larger than 0°, the shapes of the nanocones significantly changed (Figs. 2a–d). Specifically, off-axis deposition leads to oblique nanocones with asymmetric profiles. They even develop a slightly elliptical base. It is noteworthy that oblique nanocones can be mistaken for right (symmetric) nanocones when imaged from the direction of the center of the holder (side views in Fig. 2b, d). Imaging the structures

Table 1
Parameters of the most symmetric nanocones with 50, 100 and 200 nm diameter, as measured from the SEM images (LYRA3, Tescan).

Diameter [nm]	Edge-to-edge gap [nm]	Tip angle [°]	Height [nm]	Notes
200	300	23.2 ± 2.6	243 ± 9	Truncated cone, flat top
100	300	26.7 ± 3.5	193 ± 19	Cone, sharp tip
50	300	28.3 ± 3.5	104 ± 11	Cone, sharp tip

from different viewing angles is thus crucial, as demonstrated by the top and front views in Fig. 2b, d, which clearly show the asymmetry. As can be presumed, the asymmetry is the largest in the case of the sample with the largest values of distance from the holder center and flux incidence angle (Fig. 2a). In this case, the nanocones are asymmetric in both views (side and front) because of a viewing direction from the holder center is located 45° between the side and front normal angles.

While most of the truly symmetric (right) nanocones have sidewall angles (left or right parts of the tip angles – schema in Fig. SD2c, Supplementary Data) around 11°–14° (leading to the mean tip angles around 22°–28°, see Table 1), some of the most asymmetric oblique nanocones have sidewall angles of 23°–24° on one side and 0°–2° on the other side (cf. Supplementary Data, Sect. 2). This notable difference leads to the asymmetry of the nanocone sidewall angles, which reaches the ratio of 20:1. The whole effect can be ascribed to the imperfect directionality of the deposition, which is conventionally described by Lambert's cosine law [43]. The observed asymmetry will vary for different crucible-holder distances, which will change a line-of-sight of the deposition. When the flux incidence angle is changed during deposition, more complicated conical shapes can be reached (more in the Supplementary Data, Sect. 3).

To extract the effect of non-normal deposition, we tested the deposition onto substrates placed exactly in the center of the sample holder, but slightly tilted with respect to the holder surface (angle 7°, see Fig. 2e). Although produced precisely at the deposition axis, oblique elliptical nanocones are formed. Similarly as in the previous cases, the oblique and truncated nanocones are formed when the thickness of the deposited material is low with respect to the nanowell diameter. Although the self-shading effect is desirable for the production of nanocones, it can be detrimental for the fabrication of planar nanostructures. Plasmonic nanodisc nanoantennas, for example, often have both lateral sizes and thicknesses below 100 nm [44]. But as the typical sidewall angle is around 25° (cf. Table 1), the bottom base of such nanodiscs can be significantly larger than the top face. When we deposited 50 nm of gold (plus 5 nm of titanium) onto 50 nm nanowells (Fig. 3), blunt truncated nanocones were formed with the top face having half the diameter of the bottom base, as apparent under the tilted view. This is considerably different from the idealized cylindrical shape, which is often assumed for the modeling of similar plasmonic nanostructures. This deviation from the ideal shape is difficult to discern from images acquired in the conventional top view. Inspection of the deposited nanostructures at multiple viewing angles by SEM is therefore highly recommended. Only that way, the true shape of the nanostructures can be assessed and later incorporated into realistic numerical simulations or theoretical calculations. Measurements of the topography using scanning probe microscopy is another option how to detect asymmetries of the structures. However, such measurements can become complicated, especially for very dense arrays and structures below 100 nm, due to quite a big aspect ratio of nanocones and limited sharpness of the probe.

The self-shading effect also enables the fabrication of more complex 3D structures than just an ordinary nanocone. The fabricated nanocones can be left embedded inside nanowells made of hardened resist if the sample is exposed to an electron beam after the metal deposition, but before the lift-off (Fig. 4a). The bridged gold nanocones in Fig. 4b could be fabricated by the patterning of a pair of circles (here with a diameter of 100 nm) connected by a line with a width smaller than the diameter of the circle (here with a width of 50 nm). Using this approach, even more complicated networks of interconnected nanocones can be fabricated (Fig. 4c), with potential applications in all sorts of electrically addressable chips. Additional information on the

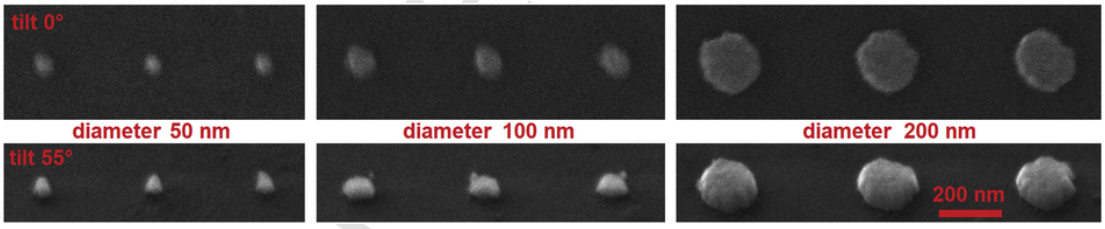

Fig. 3. SEM micrographs (MIRA3, LYRA3, Tescan) of 55 nm thick gold nanodiscs with a diameter of (left) 50 nm, (center) 100 nm, and (right) 200 nm. (Top row) top view SEM with the 0° tilt, (bottom row) SEM view with the 55° tilt.

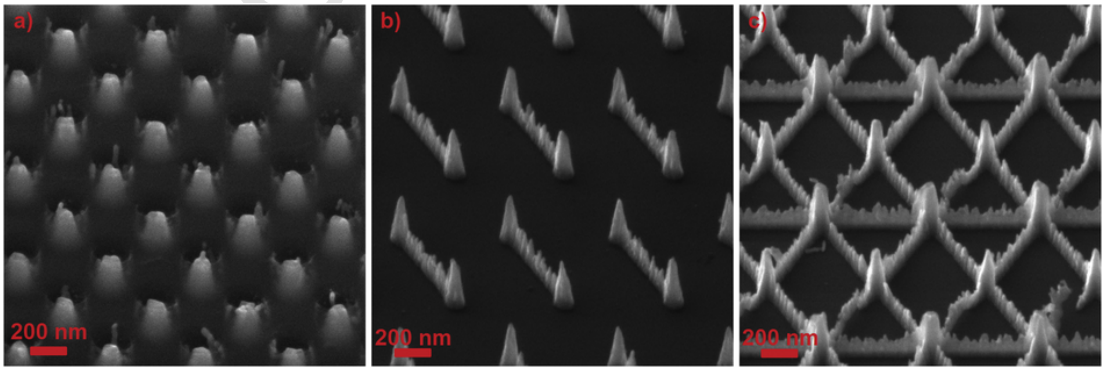

Fig. 4. SEM micrographs (LYRA3, Tescan) under the 55° tilt of: (a) truncated nanocones inside hardened resist nanowells, (b) pairs of bridged nanocones, (c) interconnected nanocones.

design and features of the interconnected nanocone arrays can be found in the Supplementary Data, Sect. 4.

4. Conclusions

In conclusion, we have shown that symmetric (right) metal nanocones can be formed by the self-shading effect only when the metal deposition direction is almost perfectly perpendicular to the sample surface. Yet this requirement is very hard to achieve in practice as even a small tilt of the sample or its lateral shift out from the sample holder center will result in deviation from perpendicular deposition in many physical vapor deposition systems. Importantly, the resulting asymmetry is hard to identify in the conventional SEM images acquired under a normal viewing angle. Failing to take asymmetries of fabricated nanostructures or that most 'cylindrical discs' fabricated by metal deposition and lift-off will indeed be truncated cones creates significant errors in the modeling of actual plasmonic nanostructures. We suggest that when fully symmetric (right circular) nanocones are desired, the deposition directionality should be well controlled and confirmed using SEM imaging at multiple viewing angles. When large areas of symmetric nanostructures are needed, one could compensate for the inherently asymmetric physical vapor deposition by non-planar sample holders. Smart utilization of the knowledge described in this study allows that interesting, robust sensing or detection platforms with 3D geometries could be created. We demonstrated such examples of nanocones inside dielectric nanowells and arrays of bridged or interconnected nanocones.

Credit author statement

All authors discussed the results and participated on the manuscript. JL: proposing the experiment, fabrication, manuscript writing, FL: management of the research, manuscript writing, PVP, PD: fabrication, LK: measurements, MK: calculations, NSL: consultations, ER, TŠ: funding acquisition and supervision.

Declaration of Competing Interest

The authors declare that they have no known competing financial interests or personal relationships that could have appeared to influence the work reported in this paper.

Acknowledgments

This research was carried out under project GA17-33767L of Grant Agency of the Czech Republic, H2020 Twinning programme (project SINNCE, 810626) and Brno University of Technology (project FSI-S-17-4482). The work was also supported by the project CEITEC 2020 (LQ1601) with financial support from the Ministry of Education, Youth and Sports of the Czech Republic under the National Sustainability Programme II. We acknowledge CzechNanoLab Research Infrastructure supported by MEYS CR (LM2018110). The research was partly funded by the Austrian Science Fund (FWF) grant number I 3064 and by the City of Vienna Hochschuljubiläumsfonds project H-268476/2016.

Appendix A. Supplementary data

Supplementary data to this article can be found online at https://doi.org/10.1016/j.mee.2020.111326.

References

[1] B.C. Stipe, T.C. Strand, C.C. Poon, H. Balamane, T.D. Boone, J.A. Katine, J.L. Li, V. Rawat, H. Nemoto, A. Hirotsune, et al., Magnetic recording at 1.5Pbm-2using an integrated plasmonic antenna, Nat. Photonics 4 (2010) 484–488, https://doi.org/10.1038/nphoton.2010.90.
[2] N. Rotenberg, L. Kuipers, Mapping nanoscale light fields, Nat. Photonics 8 (2014) 919–926, https://doi.org/10.1038/nphoton.2014.285.
[3] V.-C. Su, C.H. Chu, G. Sun, D.P. Tsai, Advances in optical metasurfaces: fabrication and applications [invited], Opt. Express 26 (2018) 13148, https://doi.org/10.1364/oe.26.013148.
[4] J.R. Mejía-Salazar, O.N. Oliveira, Plasmonic biosensing, Chem. Rev. 118 (2018) 10617–10625, https://doi.org/10.1021/acs.chemrev.8b00359.
[5] M. Mayer, M.J. Schnepf, T.A.F. König, A. Fery, Colloidal self-assembly concepts for plasmonic metasurfaces, Adv. Opt. Mater. 1800564 (2018) 1–17, https://doi.org/10.1002/adom.201800564.
[6] J.T. Collins, C. Kuppe, D.C. Hooper, C. Sibilia, M. Centini, V.K. Valev, Chirality and chiroptical effects in metal nanostructures: fundamentals and current trends, Adv. Opt. Mater. 5 (2017) 1–46, https://doi.org/10.1002/adom.201700182.
[7] R. Hensel, K. Moh, E. Arzt, Engineering micropatterned dry adhesives: from contact theory to handling applications, Adv. Funct. Mater. 28 (2018) 1800865, https://doi.org/10.1002/adfm.201800865.
[8] G. Das, E. Battista, G. Manzo, F. Causa, P.A. Netti, E. Di Fabrizio, Large-scale Plasmonic NanoCones array for spectroscopy detection, ACS Appl. Mater. Interfaces 7 (2015) 23597–23604, https://doi.org/10.1021/acsami.5b06887.
[9] Y. Oh, M. Kang, M. Park, K. Jeong, Engineering hot spots on plasmonic nanopillar arrays for SERS: a review, BioChip J. 10 (2016) 297–309, https://doi.org/10.1007/s13206-016-0406-2.
[10] L.P. Hackett, L.L. Goddard, G.L. Liu, Plasmonic nanocone arrays for rapid and detailed cell lysate surface enhanced Raman spectroscopy analysis, Analyst 142 (2017) 4422–4430, https://doi.org/10.1039/c7an00630f.
[11] J. Fulmes, R. Jäger, A. Bräuer, C. Schäfer, S. Jäger, D.A. Gollmer, A. Horrer, E. Nadler, T. Chassé, D. Zhang, et al., Self-aligned placement and detection of quantum dots on the tips of individual conical Plasmonic nanostructures, Nanoscale 7 (2015) 14691–14696, https://doi.org/10.1039/c5nr03546e.
[12] M. Fleischer, C. Stanciu, F. Stade, J. Stadler, K. Braun, A. Heeren, M. Häffner, D.P. Kern, A.J. Meixner, Three-dimensional optical antennas: nanocones in an apertureless scanning near-field microscope, Appl. Phys. Lett. 93 (2008) 3–5, https://doi.org/10.1063/1.2987485.
[13] M. Fleischer, F. Stade, A. Heeren, M. Häffner, K. Braun, C. Stanciu, R. Ehlich, J.K.H. Hörber, A.J. Meixner, D.P. Kern, Nanocones on transparent substrates for investigations in scanning probe microscopes, Microelectron. Eng. 86 (2009) 1219–1221, https://doi.org/10.1016/j.mee.2008.11.091.
[14] M. Fleischer, A. Weber-Bargioni, M.V.P. Altoe, A.M. Schwartzberg, P.J. Schuck, S. Cabrini, D.P. Kern, Gold nanocone near-field scanning optical microscopy probes, ACS Nano 5 (2011) 2570–2579, https://doi.org/10.1021/nn102199u.
[15] K. Kumar, A.B. Dahlin, T. Sannomiya, S. Kaufmann, L. Isa, E. Reimhult, Embedded plasmonic nanomenhirs as location-specific biosensors, Nano Lett. 13 (2013) 6122–6129, https://doi.org/10.1021/nl403445f.
[16] V. Claudio, A.B. Dahlin, T.J. Antosiewicz, Single-particle plasmon sensing of discrete molecular events: binding position versus signal variations for different sensor geometries, J. Phys. Chem. C 118 (2014) 6980–6988, https://doi.org/10.1021/jp412219v.
[17] J. Fulmes, C. Schäfer, D.P. Kern, P.M. Adam, M. Fleischer, Relative spectral tuning of the vertical versus base modes in plasmonic nanocones, Nanotechnology 30 (2019) 20–22, https://doi.org/10.1088/1361-6528/ab2d5c.
[18] R.M. Córdova-Castro, A.V. Krasavin, M.E. Nasir, A.V. Zayats, W. Dickson, Nanocone-based plasmonic metamaterials, Nanotechnology 30 (2019)055301https://doi.org/10.1088/1361-6528/aaea39.
[19] F. De Angelis, C. Liberale, M.L. Coluccio, G. Cojoc, E. Di Fabrizio, Emerging fabrication techniques for 3D Nano-structuring in plasmonics and single molecule studies, Nanoscale 3 (2011) 2689–2696, https://doi.org/10.1039/c1nr10124b.
[20] B. Hoffmann, S. Vassant, X.-W. Chen, S. Götzinger, V. Sandoghdar, S. Christiansen, Fabrication and characterization of plasmonic nanocone antennas for strong spontaneous emission enhancement, Nanotechnology 26 (2015) 404001, https://doi.org/10.1088/0957-4484/26/40/404001.
[21] K. Matsuzaki, S. Vassant, H.-W. Liu, A. Dutschke, B. Hoffmann, X. Chen, S. Christiansen, M.R. Buck, J.A. Hollingsworth, S. Götzinger, et al., Strong plasmonic enhancement of biexciton emission: controlled coupling of a single quantum dot to a gold Nanocone antenna, Sci. Rep. 7 (2017) 42307, https://doi.org/10.1038/srep42307.
[22] A.M. Flatae, F. Tantussi, G.C. Messina, A. Mohammadi, F. De Angelis, M. Agio, Plasmonic gold Nanocones in the near-infrared for quantum nano-optics, Adv. Opt. Mater. 5 (2017) 1700586, https://doi.org/10.1002/adom.201700586.
[23] H. Fredriksson, Y. Alaverdyan, A. Dmitriev, C. Langhammer, D.S. Sutherland, M. Zäch, B. Kasemo, Hole-Mask colloidal lithography, Adv. Mater. 19 (2007) 4297–4302, https://doi.org/10.1002/adma.200700680.
[24] C.M. Hsu, S.T. Connor, M.X. Tang, Y. Cui, Wafer-scale silicon nanopillars and nanocones by Langmuir-Blodgett assembly and etching, Appl. Phys. Lett. 93 (2008) 13–15, https://doi.org/10.1063/1.2988893.
[25] F. Stade, A. Heeren, M. Fleischer, D.P. Kern, Fabrication of metallic nanostructures for investigating Plasmon-induced field enhancement, Microelectron. Eng. 84 (2007) 1589–1592, https://doi.org/10.1016/j.mee.2007.01.256.
[26] M. Toma, G. Loget, R.M. Corn, Fabrication of broadband antireflective plasmonic gold nanocone arrays on flexible polymer films, Nano Lett. 13 (2013) 6164–6169, https://doi.org/10.1021/nl403496a.
[27] L. Mehrvar, M. Sadeghipari, S.H. Tavassoli, S. Mohajerzadeh, M. Fathipour, Optical and surface enhanced Raman scattering properties of Ag modified silicon double

nanocone array, Sci. Rep. 7 (2017) 1–13, https://doi.org/10.1038/s41598-017-12423-2.
[28] M. Fleischer, D. Zhang, K. Braun, S. Jäger, R. Ehlich, M. Häffner, C. Stanciu, J.K.H.H. Hörber, A.J. Meixner, D.P. Kern, Tailoring gold nanostructures for near-field optical applications, Nanotechnology 21 (2010)065301https://doi.org/10.1088/0957-4484/21/6/065301.
[29] B. Ai, L. Wang, H. Möhwald, Y. Yu, G. Zhang, Asymmetric half-cone/nanohole array films with structural and directional reshaping of extraordinary optical transmission, Nanoscale 6 (2014) 8997–9005, https://doi.org/10.1039/c4nr01385a.
[30] Z. Wang, B. Ai, Z. Zhou, Y. Guan, H. Möhwald, G. Zhang, Free-standing plasmonic chiral metamaterials with 3D resonance cavities, ACS Nano 12 (2018) 10914–10923, https://doi.org/10.1021/acsnano.8b04106.
[31] M. Kölbel, R.W. Tjerkstra, J. Brugger, C.J.M. Van Rijn, W. Nijdam, J. Huskens, D.N. Reinhoudt, Shadow-mask evaporation through monolayer-modified Nanostencils, Nano Lett. 2 (2002) 1339–1343, https://doi.org/10.1021/nl025784o.
[32] L. Isa, K. Kumar, M. Müller, J. Grolig, M. Textor, E. Reimhult, Particle lithography from colloidal self-assembly at liquid–liquid interfaces, ACS Nano 4 (2010) 5665–5670, https://doi.org/10.1021/nn101260f.
[33] M. Tabatabaei, M. Najiminaini, K. Davieau, B. Kaminska, M.R. Singh, J.J.L. Carson, F. Lagugné-Labarthet, Tunable 3D Plasmonic cavity nanosensors for surface-enhanced Raman spectroscopy with sub-Femtomolar limit of detection, ACS Photonics 2 (2015) 752–759, https://doi.org/10.1021/acsphotonics.5b00104.
[34] Y. Zhao, G. Gaur, R.L. Mernaugh, P.E. Laibinis, S.M. Weiss, Comparative kinetic analysis of closed-ended and open-ended porous sensors, Nanoscale Res. Lett. 11 (2016) 395, https://doi.org/10.1186/s11671-016-1614-3.
[35] A.R. Ferhan, J.A. Jackman, B. Malekian, K. Xiong, G. Emilsson, S. Park, A.B. Dahlin, N.-J. Cho, Nanoplasmonic sensing architectures for decoding membrane curvature-dependent biomacromolecular interactions, Anal. Chem. 90 (2018) 7458–7466, https://doi.org/10.1021/acs.analchem.8b00974.
[36] J.M. Kontio, H. Husu, J. Simonen, M.J. Huttunen, J. Tommila, M. Pessa, M. Kauranen, Nanoimprint fabrication of gold nanocones with ~10 nm tips for enhanced optical interactions, Opt. Lett. 34 (2009) 1979, https://doi.org/10.1364/OL.34.001979.
[37] J.M. Kontio, J. Simonen, J. Tommila, M. Pessa, Arrays of metallic nanocones fabricated by UV-nanoimprint lithography, Microelectron. Eng. 87 (2010) 1711–1715, https://doi.org/10.1016/j.mee.2009.08.015.
[38] W. Wu, M. Hu, F.S. Ou, Z. Li, R.S. Williams, Cones fabricated by 3D nanoimprint lithography for highly sensitive surface enhanced Raman spectroscopy, Nanotechnology 21 (2010) 1–6, https://doi.org/10.1088/0957-4484/21/25/255502.
[39] J. Zhao, W. Sun, W. Sun, L. Liu, X. Xia, B. Quan, A. Jin, C. Gu, J. Li, Rapid templated fabrication of large-scale, high-density metallic nanocone arrays and SERS applications, J. Mater. Chem. C 2 (2014) 9987–9992, https://doi.org/10.1039/c4tc01338g.
[40] Y. Liu, K. Du, I. Wathuthanthri, C.-H. Choi, From nanocone to nanodisc: structural transformation of gold nanoarrays via simple mechanical stresses, J. Vac. Sci. Technol. B Nanotechnol. Microelectron. Mater. Process. Meas. Phenom. 30 (2012)06FF10https://doi.org/10.1116/1.4765635.
[41] S. Rao, M.J. Huttunen, J.M. Kontio, J. Makitalo, M.-R. Viljanen, J. Simonen, M. Kauranen, D. Petrov, Tip-enhanced Raman scattering from bridged Nanocones, Opt. Express 18 (2010) 23790, https://doi.org/10.1364/oe.18.023790.
[42] M.J. Huttunen, K. Lindfors, D. Andriano, J. Mäkitalo, G. Bautista, M. Lippitz, M. Kauranen, Three-dimensional winged nanocone optical antennas, Opt. Lett. 39 (2014) 3686, https://doi.org/10.1364/OL.39.003686.
[43] H. Frey, H.R. Khan, Handbook of Thin-Film Technology, Springer, 2015.
[44] J. Babocký, A. Křížová, L. Štrbková, L. Kejík, F. Ligmajer, M. Hrtoň, P. Dvořák, M. Týč, J. Čolláková, V. Křápek, et al., Quantitative 3D phase imaging of plasmonic metasurfaces, ACS Photonics 4 (2017) 1389–1397, https://doi.org/10.1021/acsphotonics.7b00022.